INTERNATIONAL JOURNAL FOR NUMERICAL METHODS IN FLUIDS
Int. J. Numer. Meth. Fluids 2009; **59**:677–690
Published online 17 June 2008 in Wiley InterScience (www.interscience.wiley.com). DOI: 10.1002/fld.1839

Viscoelastic effects in double-pipe single-pass counterflow heat exchangers

T. Chinyoka*, †

Center for Advanced Studies in Mathematics, Lahore University of Management Sciences, 54792 Lahore, Pakistan

SUMMARY

The conducto-convective heat loss from a viscoelastic liquid, in the core of a double-pipe heat exchanger arrangement, to a cooler Newtonian fluid flowing in the outer annulus is investigated with direct numerical simulations. A numerical algorithm based on the finite difference method is implemented in time and space with the Giesekus constitutive model for the viscoelastic liquids. The flow of both the annulus and core-fluids is considered to be Poiseuille flow, driven by respective pressure gradients. In general, the results show that a viscoelastic core-fluid leads to slightly lower (albeit comparable) attainable temperatures in the core-fluid stream as compared with a corresponding Newtonian fluid. Copyright © 2008 John Wiley & Sons, Ltd.

Received 2 March 2007; Revised 15 March 2008; Accepted 17 March 2008

KEY WORDS: counterflow; heat exchanger; viscoelastic liquid; Giesekus model

1. INTRODUCTION

The study of *direct transfer-type heat exchangers* (*recuperators*) that do not allow for the mixing of the hot and cold fluid streams is a model problem in the food-processing industry among other industrial heating and cooling applications [1–5]. In the food-processing industry, the need usually arises for the heating and cooling of liquid foods, the categorization/flow of which is generally non-Newtonian by nature. However, the theoretical literature on the non-Newtonian effects in such pertinent and modern heat exchanger designs is very sparse and this provides the impetus for the current investigation. A good overview of related literature is given, say in [6], for the helical double-pipe heat exchangers, and in [7, 8], for shell-and-tube heat exchangers.

*Correspondence to: T. Chinyoka, Department of Mathematics and Applied Mathematics, University of Cape Town, Private Bag Rondebosch 7701, South Africa.
†E-mail: tchinyok@vt.edu

Contract/grant sponsor: Center for Advanced Studies in Mathematics

For a comprehensive overview of non-Newtonian flows in general and viscoelastic fluid phenomena in particular, we refer to the excellent treatises of [9, 10]. A development of the energy equations for various viscoelastic flows is well documented in [11]. Detailed discussions of the interrelationships between heat transfer mechanisms and polymeric fluid characteristics are also outlined therein.

For single-pass heat exchangers, the counterflow arrangement is most thermodynamically superior to any of the other possible flow arrangements (i.e. cross flow and parallel flow) [1, 3–5]. In particular, the counterflow arrangement is the most efficient in producing the highest temperature change in each fluid compared with any other two-fluid recuperator arrangement for a given overall thermal conductance, fluid flow rates and flow inlet temperatures. Moreover, the maximum temperature difference across the exchanger wall thickness either at the hot- or cold-fluid end is the lowest and produces minimum thermal stresses in the wall for an equivalent performance compared with either the cross flow or the parallel flow arrangements. It is thus also in light of these observations that we choose to limit our study to the counterflow heat exchanger.

In Section 2 we present the model problem and its governing equations. We proceed in Section 3 to develop the numerical algorithm that will be used to solve the respective set of equations. The main results of the current work, implementing viscoelastic models for the core-fluid, are presented in Section 4. Concluding remarks follow in Section 5.

2. MATHEMATICAL MODELING

Figure 1 is a sketch of the two-dimensional model problem. The model consists of an inner channel (which we shall refer to as the core) symmetrically surrounded by outer channels (which form the shell of what are broadly referred to as shell-and-tube heat exchangers). The core has dimensions $L^* \times (\varepsilon_c L^*)$ and the shell has the same length L^* but width $\varepsilon_s L^*$, where $0<\varepsilon_s, \varepsilon_c \leqslant 1$. The superscript $*$ will denote a dimensional quantity.

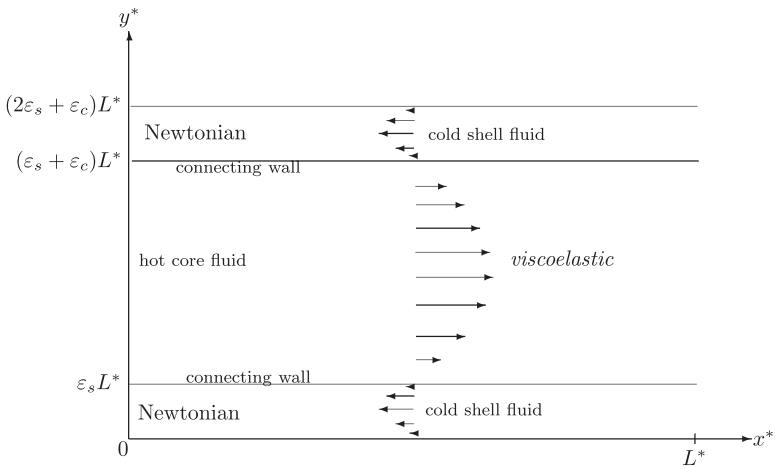

Figure 1. Schematics of the model problem.

DOI: 10.1002/fld

In the counterflow setup pertinent to this investigation, the core-fluid moves from left to right driven by a negative pressure gradient $-G_c^*$ in the x-direction and the shell-fluid flows in the opposite direction in response to the positive pressure gradient G_s^*. We will, respectively, adopt the subscripts c and s to denote core- and shell-fluid quantities and in the same vein, we will denote the dimensional temperature of the connecting wall by $T_w^*(t,x)$.

We will assume that the core-fluid is a viscoelastic liquid subjected to two-dimensional flow velocity. Compared with the core, we suppose that the shell is a much narrower section and allows for a one-dimensional flow assumption of the Newtonian fluid flowing therein. The boundary conditions for the velocity, $\mathbf{u}^*=(u^*,v^*)$, are prescribed at the horizontal solid walls (no-slip and wall impermeability) and at the channel inlets. The conditions at the channel outlets will be determined as the solution process progresses. In particular, we linearly extrapolate the neighborhood values to obtain these. Corresponding values for the other flow variables (temperature, T_c^*, T_s^*; core pressure, p_c^*; and extra stresses, $\underline{\underline{\tau}}^*$) on the unprescribed boundaries will be similarly reconstructed from the main flow. The temperature and pressure will be prescribed at the channel inlets.

The coefficients of thermal expansion, convective heat transfer coefficients, specific heat capacities, densities and thermal conductivities of the fluids will be taken as constant and denoted as $c_{\beta_c}^*, c_{\beta_s}^*$, h_c^*, h_s^*, $c_{p_c}^*$, $c_{p_s}^*$, ρ_c^*, ρ_s^*, and κ_c^*, κ_s^*, respectively. On the other hand, the viscosities and relaxation time will be assumed in general to depend on temperature and will be denoted as follows. For the core-fluid, relaxation time is $\lambda^*(T_c^*)$, solvent viscosity is $\eta_{\mathrm{sol}}^*(T_c^*)$, polymeric viscosity is $\eta_p^*(T_c^*)$ and total viscosity is $\eta_c^*(T_c^*)=\eta_{\mathrm{sol}}^*(T_c^*)+\eta_p^*(T_c^*)$. In the shell-fluid, the total viscosity is the same as its solvent viscosity and is denoted by $\eta_s^*(T_s^*)$.

2.1. Governing equations for core-fluid

The core-fluid system is governed by the continuity, momentum and energy equations for incompressible viscoelastic fluids:

$$\nabla^*\cdot\mathbf{u}_c^*=0$$

$$\rho_c\frac{\mathrm{D}\mathbf{u}_c^*}{\mathrm{D}t^*}=\nabla^*\cdot\underline{\underline{\sigma}}_c^*+\mathbf{F}_c^*$$

$$\rho_c^* c_{p_c}^*\frac{\mathrm{D}T_c^*}{\mathrm{D}t^*}=Q_{D\mathrm{c}}^*-\nabla^*\cdot\mathbf{\Phi}_{q_c}^*+c_{\beta_\mathrm{c}}^* T_c^*\mathbf{u}_c^*\cdot\nabla p_c^*+h_c^*(T_w^*-T_c^*)$$

where $\mathbf{F}_c^*$ is the body force due to fouling/friction factors and will henceforth be neglected. The total stress tensor is $\underline{\underline{\sigma}}_c^*=-p_c^*\underline{\underline{I}}+\underline{\underline{\tau}}^*+\eta_c^*\underline{\underline{S}}_c^*$, where $\underline{\underline{S}}_c^*=[\nabla^*\mathbf{u}_\mathbf{c}^*+(\nabla^*\mathbf{u}_\mathbf{c}^*)^{\mathrm{T}}]$ is the deformation rate tensor, $\underline{\underline{I}}$ is the unit tensor and $\underline{\underline{\tau}}^*$ is the extra stress tensor. $Q_{Dc}^*=\gamma\underline{\underline{\tau}}^*:\underline{\underline{S}}_c^*+(1-\gamma)\eta_{\mathrm{sol}}^*\underline{\underline{S}}_c^*:\underline{\underline{S}}_c^*$ is the internal heat production consisting of an irreversible part $\eta_{\mathrm{sol}}^*\underline{\underline{S}}_c^*:\underline{\underline{S}}_c^*$ called the mechanical dissipation and a reversible part $\underline{\underline{\tau}}^*:\underline{\underline{S}}_c^*$. The symbol ':' is the double dot product of two tensors, γ is a weighting constant for the dissipative terms such that $0\leqslant\gamma\leqslant1$. $\mathrm{D}/\mathrm{D}t^*$ is the material derivative and $\mathbf{\Phi}_{q_c}^*$ is the heat flux.

We will model the temperature dependence of the relaxation time and viscosities by a Nahme-type law [12, 13]:

$$\lambda^*=\lambda_0\bar{\lambda}(T_c^*),\quad \eta_{\mathrm{sol}}^*=\eta_{\mathrm{sol}_0}\mu_c(T_c^*),\quad \eta_p^*=\eta_{p_0}\mu_c(T_c^*),\quad \eta_s^*=\eta_{s_0}\mu_c(T_c^*)$$

DOI: 10.1002/fld

where

$$\bar{\lambda}(T_c^*)=(1-\delta_\lambda)+\delta_\lambda\frac{T_{c_0}^*}{T_c^*}\exp(-\varepsilon_\lambda\Theta_c),\quad \mu_c(T_c^*)=\exp(-\varepsilon_\eta\Theta_c)$$

with $\Theta=(T_c^*-T_{c_0})/(\Delta T^*)$ and $\Delta T^*=T_{c_0}^*-T_{s_0}^*$. All quantities subscripted by zero are constant reference values and $\delta_\lambda\in\{0,1\}$ is a delta function such that

$$\delta_\lambda=\begin{cases}0 & \text{if } \varepsilon_\lambda=0\\ 1 & \text{otherwise}\end{cases}$$

The heat flux is given by Fourier's law $\mathbf{\Phi}_{q_c}^*=-\kappa_c^*\nabla^*T_c^*$ and we use the non-isothermal Giesekus model for the extra stress tensor $\underline{\underline{\tau}}^*$ [14, 15];

$$\underline{\underline{\tau}}^*+\alpha^*\underline{\underline{\tau}}^{*2}+\lambda^*\left(\overset{\nabla}{\underline{\underline{\tau}}}{}^*-\underline{\underline{\tau}}^*\frac{\mathrm{D}}{\mathrm{D}t^*}(\ln[T_c^*/T_{s_0}^*])\right)=\eta_p^*(T_c^*)\underline{\underline{S}}_v^*$$

where the upper convected time derivative $\overset{\nabla}{\underline{\underline{\tau}}}{}^*$ is defined as

$$\overset{\nabla}{\underline{\underline{\tau}}}{}^*=\frac{\partial\underline{\underline{\tau}}^*}{\partial t^*}+(\mathbf{u}_\mathbf{c}^*\cdot\nabla^*)\underline{\underline{\tau}}^*-(\nabla^*\mathbf{u}_\mathbf{c}^*)\underline{\underline{\tau}}^*-\underline{\underline{\tau}}^*(\nabla^*\mathbf{u}_\mathbf{c}^*)^{\mathrm{T}}$$

If we denote by $U_{c_0}^*$ the maximum velocity along the centerline of the channel, then the dimensionless parameters for the problem are

$$Re_c=\frac{\rho_c^*U_{c_0}^*L^*}{\eta_{c_0}^*},\quad De=\frac{\lambda_0^*U_{c_0}^*}{L^*},\quad Pr_c=\frac{c_{p_c}^*\eta_{c_0}^*}{\kappa_c^*},\quad \beta=\frac{\eta_{p_0}^*}{\eta_{c_0}^*}$$

$$h_c=\frac{L^{*2}}{\kappa^*}h_c^*,\quad \delta_{c_3}=c_{\beta_c}^*T_{c_0}^*,\quad \delta_{c_2}=\frac{\eta_{c_0}^*U_{c_0}^{*2}}{\kappa_c^*\Delta T^{*2}},\quad \alpha=\frac{L^*}{\eta_{c_0}^*\mu_cU_{c_0}^*}\alpha^*$$

Here Re_c, De and Pr_c are, respectively, the Reynolds, Deborah and Prandtl numbers, β is the ratio of the polymer to total viscosity, h_c is the convective heat transfer parameter, δ_{c_2} is connected with dissipative effects, δ_{c_3} is a thermal expansion parameter and α is the Giesekus nonlinear parameter. If we next introduce the dimensionless variables

$$t=\frac{U_{c_0}^*}{L^*}t^*,\quad \mathbf{x}=\frac{\mathbf{x}^*}{L^*},\quad \mathbf{u}_c=\frac{\mathbf{u}_c^*}{U_{c_0}^*},\quad p_c=\rho^*U_{c_0}^{*2}p_c^*,\quad T_c=\frac{(T_c^*-T_{s_0}^*)}{\Delta T^*}$$

$$\bar{\lambda}=\frac{\lambda^*}{\lambda_0^*},\quad \mu_c=\frac{\eta_c^*}{\eta_{c_0}^*},\quad \nabla=L^*\nabla^*,\quad \underline{\underline{\tau}}=\frac{L^*}{\eta_c^*U_{c_0}^*}\underline{\underline{\tau}}^*,\quad \underline{\underline{S}}_c=\frac{L^*}{U_{c_0}^*}\underline{\underline{S}}_c^*$$

then the dimensionless governing equations for the velocity, temperature and stress components are as given in Equations (1)–(4):

$$\nabla\cdot\mathbf{u}_c=0 \tag{1}$$

$$\frac{\mathrm{D}\mathbf{u}_c}{\mathrm{D}t}=-\nabla p_c+\frac{1}{Re_c}\nabla\cdot[(\mu_c\underline{\underline{\tau}})+(\mu_c\underline{\underline{S}}_c)] \tag{2}$$

DOI: 10.1002/fld

$$Re_c Pr_c \frac{\mathrm{D}T_c}{\mathrm{D}t} = \nabla^2 T_c + \delta_{c_2}\mu_c[\gamma(\underline{\underline{\tau}}:\underline{\underline{S}}_c) + (1-\gamma)(1-\beta)\underline{\underline{S}}_c:\underline{\underline{S}}_c]$$

$$+Re_c\,\delta_{c_2}\delta_{c_3}\left(T_c+\frac{1}{\xi}\right)\mathbf{u}_c\cdot\nabla p_c + h_c(T_w - T_c) \tag{3}$$

$$\underline{\underline{\tau}} + \alpha\underline{\underline{\tau}}^2 + De\frac{\bar{\lambda}}{\mu_c}\left([\overset{\nabla}{\mu_c\underline{\underline{\tau}}}] - \mu_c\underline{\underline{\tau}}\frac{\mathrm{D}}{\mathrm{D}t}\ln[\xi T_c + 1]\right) = \beta\underline{\underline{S}} \tag{4}$$

where

$$\xi = \frac{\Delta T}{T_{s_0}}, \quad \mu_c = \exp(-\varepsilon_\eta T_c), \quad \bar{\lambda} = (1-\delta_\lambda) + \delta_\lambda\frac{1+\xi}{(1+\xi T_c)}\exp(-\varepsilon_\lambda T_c)$$

The dimensionless basic velocity $(U_c(y), 0)$ is the same as for the Newtonian Poiseuille flow case:

$$U_c(y) = -\frac{G_c Re_c}{2\mu_c}(y^2 - y) \tag{5}$$

where $G_c = G_c^* L^*/(\rho_c^* U_{c_0}^{*2})$ is the dimensionless pressure gradient [16]. Following [16], we take the basic extra stress tensor as

$$\underline{\underline{\tau}} = \begin{pmatrix} C_1 & C_2 \\ C_2 & 0 \end{pmatrix}, \quad C_1 = 2De\frac{(1-\beta)}{Re_c}[U_c'(y)]^2, \quad C_2 = 2\frac{(1-\beta)}{Re_c}U_c'(y)$$

An alternative condition with $C_1 = C_2 \equiv 0$ gives similar results.

2.2. *Governing equations for shell-fluid*

The shell-fluid system is assumed Newtonian with negligible transverse velocity $\mathbf{u}_s = (u_s(y), 0)$. The relevant governing equations thus follow from those derived for the core-fluid by neglecting the transverse velocity, v_s, transverse pressure variations $\partial p_s/\partial y = 0$ and extra stress terms, $\underline{\underline{\tau}}$. The dimensionless governing equations for the velocity and temperature are thus

$$\frac{\partial}{\partial x}u_s = 0$$

$$\frac{\partial u_s}{\partial t} + u_s\frac{\partial u_s}{\partial x} = -G_s + \frac{1}{Re_s}\left[2\frac{\partial}{\partial x}\left(\mu_s\frac{\partial u_s}{\partial x}\right) + \frac{\partial}{\partial y}\left(\mu_s\frac{\partial u_s}{\partial y}\right)\right]$$

$$Re_s Pr_s\left(\frac{\partial T_s}{\partial t} + u_s\frac{\partial T_s}{\partial x}\right) = \frac{\partial^2 T_s}{\partial x^2} + \frac{\partial^2 T_s}{\partial y^2} + 2\delta_{s_2}\mu_s\left[2\left(\frac{\partial u_s}{\partial x}\right)^2 + \left(\frac{\partial u_s}{\partial y}\right)^2\right]$$

$$+Re_s\delta_{s_2}\delta_{s_3}\left(T_s+\frac{1}{\xi}\right)u_s G_s + h_s(T_w - T_s)$$

DOI: 10.1002/fld

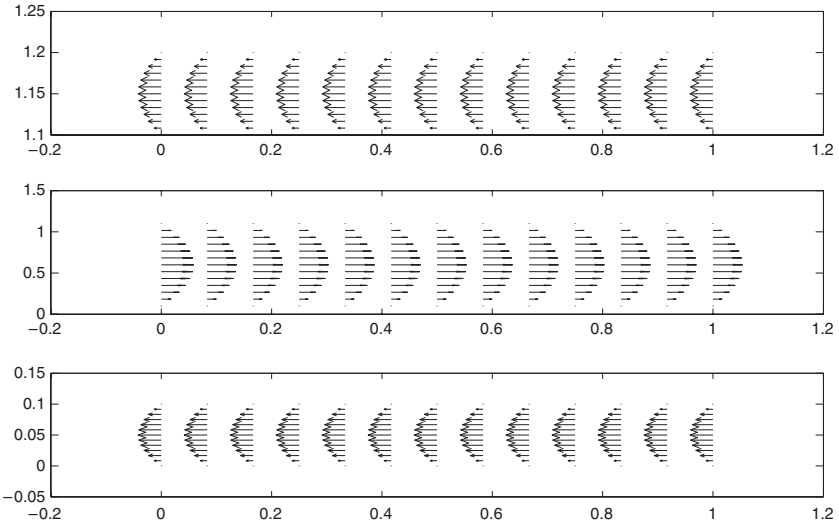

Figure 2. Scaled velocity vectors of the initial condition.

where $G_s = G_s^* L^*/(\rho_s^* U_{s_0}^{*2})$ is the dimensionless pressure gradient for the shell-fluid. The other parameters subscripted by s are similarly defined by taking analogies with corresponding core-fluid parameters. The dimensionless basic velocity $(U_s(y), 0)$ is also the same as for the Newtonian case:

$$U_s(y) = \frac{G_s Re_s}{2\mu_s}(y^2 - y) \tag{6}$$

The velocity vector plots corresponding to the initial conditions (5) and (6) are displayed in Figure 2. Here, we used $G_c = G_s = \varepsilon_s = 1$, $Re_c = 0.3$, $Re_s = 150$, where the higher Reynolds number is used in order to keep the time-steps (for the subsequent iterations) low, and for clarity we employed a rough 12×12 mesh grid.

2.3. Governing equations for connecting wall

The temperature in the connecting wall, separating the core-fluid from the shell-fluid, is governed by the one-dimensional heat conduction equation:

$$\frac{\partial T_w^*}{\partial t^*} = \kappa_w^* \frac{\partial^2 T_w^*}{\partial x^{*2}} + h_c^*(T_c^* - T_w^*) + h_s^*(T_s^* - T_w^*)$$

Using the dimensionless variables defined earlier but with $t = \kappa_w^* t^*/L^{*2}$ instead, we get the dimensionless wall temperature equation:

$$\frac{\partial T_w}{\partial t} = \frac{\partial^2 T_w}{\partial x^2} + h_c(T_c - T_w) + h_s(T_s - T_w)$$

DOI: 10.1002/fld

The boundary conditions at $x=0$ and 1 are

$$T_w|_{x=0,1}=\{[h_cT_c+h_sT_s]_{y=0.1}/(h_c+h_s)\}_{x=0,1}$$

3. NUMERICAL ALGORITHM

Our numerical algorithm is based on the semi-implicit finite difference scheme similar to that developed in [17–20] for the isothermal viscoelastic case. We modify it here to a Crank–Nicolson-type treatment of the implicit terms and also extend the algorithm to the temperature equation.

The discretization of the governing equations is based on a rectangular Cartesian mesh and uniform grid on which finite differences are taken. We approximate both the second and first spatial derivatives with second-order central differences. The equations corresponding to the first and last grid point are modified to incorporate the boundary conditions.

3.1. Numerical scheme for core region

Suppose the solution at the nth time-step is known. The numerical solution for the next time-step begins with the projection method for the momentum equation (2) which decouples the pressure computation [21].

Let $\bar{\mathbf{u}}_c$ denote the intermediate velocity field that needs to be calculated in the projection method. The semi-implicit time-integration scheme of Li [19] is applied to decouple the computation of the components of $\bar{\mathbf{u}}_c=(\bar{u}_c,\bar{v}_c)$:

$$\frac{\bar{u}_c-u_c^{(n)}}{\Delta t}=-(\mathbf{u}_c^{(n)}\cdot\nabla)u_c^{(n)}+\frac{1}{Re_c}\left(\nabla\cdot(\mu_c\underline{\underline{\tau}}_1)+2\frac{\partial\mu_c}{\partial x}\frac{\partial u_c}{\partial x}+\frac{\partial\mu_c}{\partial y}\frac{\partial u_c}{\partial y}+\frac{\partial}{\partial y}\left(\mu_c\frac{\partial v_c}{\partial x}\right)\right)^{(n)}$$
$$+\frac{1}{2}\left(\frac{\mu_c}{Re_c}\left(2\frac{\partial^2\bar{u}_c}{\partial x^2}+\frac{\partial^2\bar{u}_c}{\partial y^2}\right)+\frac{\mu_c}{Re_c}\left(2\frac{\partial^2u_c^{(n)}}{\partial x^2}+\frac{\partial^2u_c^{(n)}}{\partial y^2}\right)\right) \tag{7}$$

$$\frac{\bar{v}_c-v_c^{(n)}}{\Delta t}=-(\mathbf{u}_c^{(n)}\cdot\nabla)v_c^{(n)}+\frac{1}{Re_c}\left(\nabla\cdot(\mu_c\underline{\underline{\tau}}_2)+\frac{\partial\mu_c}{\partial x}\frac{\partial v_c}{\partial x}+2\frac{\partial\mu_c}{\partial y}\frac{\partial v_c}{\partial y}+\frac{\partial}{\partial x}\left(\mu_c\frac{\partial u_c}{\partial y}\right)\right)^{(n)}$$
$$+\frac{1}{2}\left(\frac{\mu_c}{Re_c}\left(\frac{\partial^2\bar{v}_c}{\partial x^2}+2\frac{\partial^2\bar{v}_c}{\partial y^2}\right)+\frac{\mu_c}{Re_c}\left(\frac{\partial^2v_c^{(n)}}{\partial x^2}+2\frac{\partial^2v_c^{(n)}}{\partial y^2}\right)\right) \tag{8}$$

where $\underline{\underline{\tau}}_k$ represents the kth column of the extra stress tensor and second-order central differences are used for all spatial derivatives. The implicit terms in the $\bar{u}_c$-equation are then

$$\left(1-\frac{\Delta t\mu_c}{Re_c}\frac{\partial^2}{\partial x^2}-\frac{\Delta t\mu_c}{2Re_c}\frac{\partial^2}{\partial y^2}\right)\bar{u}_c=\text{explicit terms}$$

This scheme allows for the decoupling of variables, which is an advantage over a fully implicit scheme, the operator on $\bar{u}_c$ factorizes;

$$\left(1-\frac{\Delta t\mu_c}{Re_c}\frac{\partial^2}{\partial x^2}\right)\left(1-\frac{\Delta t\mu_c}{2Re_c}\frac{\partial^2}{\partial y^2}\right)\bar{u}_c=\text{explicit terms} \tag{9}$$

DOI: 10.1002/fld

with an associated error of $O((\Delta t/Re_c)^2)$. An analogous system is solved for $\bar{v}_c$. Hence, the solution procedure for $\bar{\mathbf{u}}_c$ reduces to inversions of tridiagonal matrices. The incompressibility condition $\nabla\cdot\mathbf{u}_c^{(n)}=\nabla\cdot\mathbf{u}_c^{(n+1)}=0$, and

$$\frac{\mathbf{u}_c^{(n+1)}-\bar{\mathbf{u}}_c}{\Delta t}=-\nabla p_c \tag{10}$$

lead to the Poisson equation for pressure:

$$\nabla\cdot\nabla p_c=\frac{\nabla\cdot\bar{\mathbf{u}}_\mathbf{c}}{\Delta t} \tag{11}$$

Multi-scale problems (such as those with a small drop in a much larger domain) would necessarily demand the use of highly refined meshes and Equation (11) would more efficiently be solved with a multigrid method. For our mesh resolutions, we solve Equation (11) via direct methods without paying too much cost in terms of computational times. The updated solution $\mathbf{u}_c^{(n+1)}$ is then found with Equation (10).

The temperature and Oldroyd-B constitutive equations are treated with an analogous semi-implicit scheme. The scheme for the temperature equation is similar to that for the velocity components in that unmixed second partial derivatives of the temperature are treated implicitly:

$$\begin{aligned}\frac{T_c^{(n+1)}-T_c^{(n)}}{\Delta t}=&-(\mathbf{u}_c^{(n)}\cdot\nabla)T_c^{(n)}\\&+\frac{1}{2Re_cPr_c}\left(\frac{\partial^2T_c^{(n+1)}}{\partial x^2}+\frac{\partial^2T_c^{(n+1)}}{\partial y^2}\right)+\frac{1}{2Re_cPr_c}\left(\frac{\partial^2T_c^{(n)}}{\partial x^2}+\frac{\partial^2T_c^{(n)}}{\partial y^2}\right)\\&+\frac{2\mu_c\delta_{c_2}}{Re_cPr_c}\left[\gamma\left(\tau_{11}\frac{\partial u_c}{\partial x}+\tau_{12}\left(\frac{\partial u_c}{\partial y}+\frac{\partial v_c}{\partial x}\right)+\tau_{22}\frac{\partial v_c}{\partial y}\right)\right.\\&\left.+(1-\gamma)(1-\beta)\left(2\left(\frac{\partial u_c}{\partial x}\right)^2+\left(\frac{\partial u_c}{\partial y}+\frac{\partial v_c}{\partial x}\right)^2+2\left(\frac{\partial v_c}{\partial y}\right)^2\right)\right]^{(n)}\\&+\frac{\delta_{c_2}\delta_{c_3}}{Pr_c}\left(T_c^{(n)}+\frac{1}{\xi}\right)\left(u_c\frac{\partial p_c}{\partial x}+v_c\frac{\partial p_c}{\partial y}\right)^{(n)}+\frac{h_c}{Re_cPr_c}(T_w^{(n)}-T_c^{(n)})\end{aligned}$$

leading to the factorization

$$\left(1-\frac{\Delta t}{2Re_cPr_c}\frac{\partial^2}{\partial x^2}\right)\left(1-\frac{\Delta t}{2Re_cPr_c}\frac{\partial^2}{\partial y^2}\right)T_c^{n+1}=\text{explicit terms} \tag{12}$$

The associated error in the factorization is $O([\Delta t/(Re_cPr_c)]^2)$. For the constitutive equation, the terms that involve spatial derivatives of the extra stress tensor are taken implicitly, as is $\underline{\underline{\tau}}$:

$$(\mu_c\tau)^{(n+1/2)}+De\bar{\lambda}\left[\frac{\partial}{\partial t}+u_c^{(n)}\frac{\partial}{\partial x}+v_c^{(n)}\frac{\partial}{\partial y}\right](\mu_c\tau)^{(n+1/2)}=\text{rhs}$$

DOI: 10.1002/fld

where

$$\mathrm{rhs}_{11}=\mu_c De\bar{\lambda}\left[2\tau_{11}\frac{\partial u_c}{\partial x}+2\tau_{12}\frac{\partial u_c}{\partial y}+\tau_{11}\frac{\mathrm{D}}{\mathrm{D}t}\ln(1+\xi T_c)\right]^{(n)}+2\mu_c\beta\frac{\partial u_c^{(n)}}{\partial x}-\mu_c\alpha[\tau_{11}^{(n)}]^2$$

$$\mathrm{rhs}_{12}=\mu_c De\bar{\lambda}\left[\tau_{11}\frac{\partial v_c}{\partial x}+\tau_{22}\frac{\partial u_c}{\partial y}+\tau_{12}\left(\frac{\partial u_c}{\partial x}+\frac{\partial v_c}{\partial y}\right)+\tau_{11}\frac{\mathrm{D}}{\mathrm{D}t}\ln(1+\xi T_c)\right]^{(n)}$$
$$+\mu_c\beta\left(\frac{\partial u_c}{\partial y}+\frac{\partial v_c}{\partial x}\right)^{(n)}-\mu_c\alpha[\tau_{12}^{(n)}]^2$$

$$\mathrm{rhs}_{22}=\mu_c De\bar{\lambda}\left[2\tau_{12}\frac{\partial v_c}{\partial x}+2\tau_{22}\frac{\partial v_c}{\partial y}+\tau_{22}\frac{\mathrm{D}}{\mathrm{D}t}\ln(1+\xi T_c)\right]^{(n)}+2\mu_c\beta\frac{\partial v_c^{(n)}}{\partial y}-\mu_c\alpha[\tau_{22}^{(n)}]^2$$

The corresponding factorization is

$$\frac{2De\bar{\lambda}+\Delta t}{2De\bar{\lambda}}\left(1+\frac{De\bar{\lambda}\Delta t}{2De\bar{\lambda}+\Delta t}u^{(n)}\frac{\partial}{\partial x}\right)\left(1+\frac{De\bar{\lambda}\Delta t}{2De\bar{\lambda}+\Delta t}v^{(n)}\frac{\partial}{\partial y}\right)(\mu_c\underline{\underline{\tau}})^{(n+1)}=\text{e.t.}\tag{13}$$

with an associated error of $O(De\bar{\lambda}(\|\mathbf{u}_c\|_{\max}\Delta t)^2/(2De\bar{\lambda}+\Delta t))$. The solution procedures reduce to inversion of tridiagonal matrices.

3.2. Numerical scheme for shell region

The numerical algorithm for the velocity and temperature equations in annulus region is similar to that for the core region except we no longer need a projection method:

$$\left(1-\frac{\Delta t\mu_s}{2Re_s}\frac{\partial^2}{\partial y^2}\right)u_s^{n+1}=\text{explicit terms}$$

$$\left(1-\frac{\Delta t}{2Re_sPr_s}\frac{\partial^2}{\partial x^2}\right)\left(1-\frac{\Delta t}{2Re_sPr_s}\frac{\partial^2}{\partial y^2}\right)T_s^{n+1}=\text{explicit terms}$$

3.3. Numerical scheme for wall temperature

We assume constant convective heat transfer coefficients and thus the governing equation for the wall temperature is fully linear. We apply the full Crank–Nicolson scheme to this

$$T_w^{n+1}=T_w^n+\Delta t\left[\frac{\partial^2}{\partial x^2}T_w^{n+1/2}+h_c(T_c^n-T_w^{n+1/2})+h_s(T_s^n-T_w^{n+1/2})\right]$$

4. COMPUTATIONAL RESULTS

4.1. Sample solutions with full SIMPLE algorithm

We first test the complete numerical algorithm (i.e. taking into account both the semi-implicit scheme and the pressure solver/correction) on a square core $\varepsilon_c=1$. Unless otherwise stated,

DOI: 10.1002/fld

we mostly consider a 40×40 mesh grid for both the core and shell regions and the following parameter list: $\alpha=1$, $G_c=G_s=1$, $\delta_{c_2}=0.3$, $\delta_{s_2}=0.2$, $\delta_{c_3}=0.15$, $\delta_{s_3}=0.08$, $De=4$, $Pr_c=0.8$, $Pr_s=3$, $Re_c=0.9$, $Re_s=150$, $\gamma=0.6$, $\beta=0.6$, $\varepsilon_\lambda=0.1$, $\varepsilon_{\eta_c}=0.1$, $\varepsilon_{\eta_s}=0.1$, $\varepsilon_s=0.1$, $\mathrm{d}t=0.0001$.

The growth of the extra-stresses is illustrated in Figure 3 in terms of the first normal stress difference $N_1=\tau_{11}-\tau_{22}$ at $t=0.2$. As the core-fluid flows downstream, it loses some of its thermal energy to the ambient environment by conduction and convection. For a viscoelastic fluid, some of this energy would have been used up in the reversible processes of deformation of the constituent polymer chains. Deformation of polymer chains takes up energy whereas their relaxation gives it out [11], thus we would expect the first normal stress difference to decrease as the fluid loses heat and hence becomes more relaxed. However, since the polymer chains may not be fully relaxed, we would expect a viscoelastic fluid to be at a much lower temperature than a corresponding Newtonian fluid. This is so since some of the thermal energy that is not dissipated to the ambient environment would (in a viscoelastic fluid) still be locked up in the inherent deformations whereas in a Newtonian fluid this un-dissipated energy would manifest itself as direct fluid temperature.

Figure 4(a) shows the variation of the wall temperature ($-\circ-$, T_w) and also the adjacent boundary temperatures for the core ($-\square-$, T_c) and shell-fluids ($-\triangle-$, T_s). Figure 4(b) shows the centerline core-fluid temperature ($-\diamond-T_c$) and (coolest-to-warmest) diagonal shell-fluid temperature ($-\nabla-T_s$). Figure 4 was plotted at $t=0.15$ on a 30×30 mesh grid.

Figure 5 illustrates the surface and contour plots of the fluid temperatures at $t=0.17$. The top and bottom subplots represent the upper and lower shell-fluid values, respectively, and the middle subplots denote the core-fluid values. As expected, we notice an increase in the shell-fluid temperature as the fluid moves further from the shell inlet and this temperature rise is more pronounced closer to the connecting wall (and hence closer to the hotter core-fluid) and less so farther away from the core-fluid. Similarly, the core-fluid temperature decreases in the downstream direction while maintaining a symmetrical profile in the transverse direction, with higher temperature in the middle of the channel. At the current parameters, the minimum temperature attained in the core-fluid is $T_{c\min}=0.00180$ and the maximum temperature attained within the shell-fluid is $T_{s\max}=0.36275$.

If we change the parameter list between Newtonian and viscoelastic values we notice that the viscoelastic case leads to slightly higher temperature losses in the core-fluid stream as conjectured

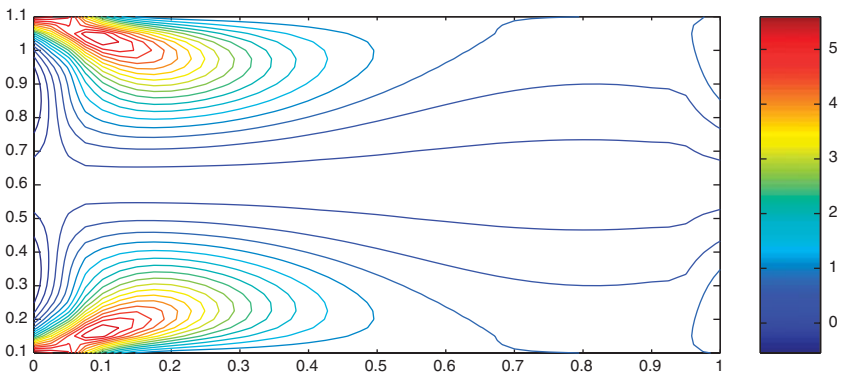

Figure 3. Contours of the first normal stress difference N_1.

DOI: 10.1002/fld

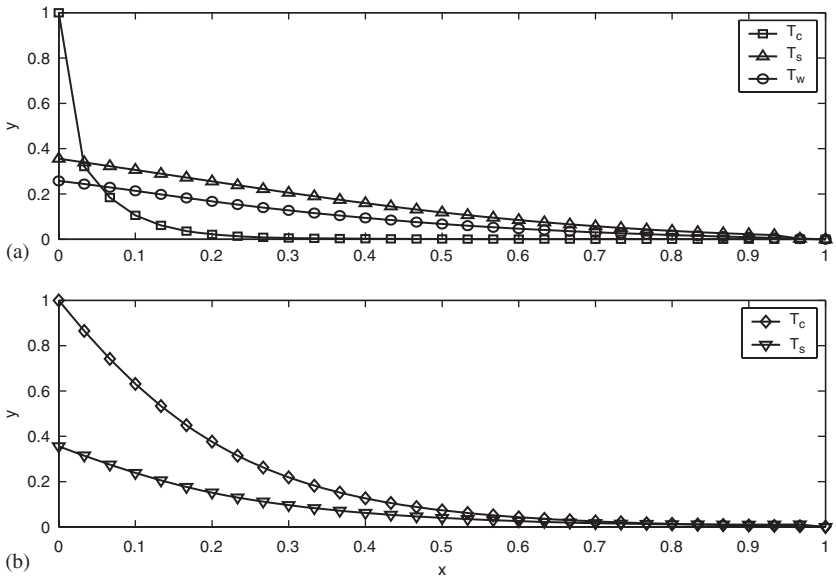

Figure 4. (a) Wall, core- and shell-fluid temperatures at the common edges and (b) mid-channel core-fluid and diagonal (coolest-to-warmest) shell-fluid temperatures.

above. For example on a 30×30 mesh grid and at $t=0.2$, a Newtonian fluid ($\alpha=De=\gamma=\beta=\varepsilon_\lambda=0$), with all other parameters as in Figure 5, leads to $T_{c\min}=0.00497$ and $T_{s\max}=0.35596$. On the other hand, a corresponding (highly elastic) Giesekus liquid ($De=4$, $\gamma=0.9$, $\beta=0.9$, $\varepsilon_\lambda=0.1$, $\alpha=1$) gives a much lower $T_{c\min}=0.000491$ and a comparable $T_{s\max}=0.35596$. An Oldroyd-B liquid (Giesekus with $\alpha\equiv0$) is intermediate with $T_{c\min}=0.00207$ and also has a comparable $T_{s\max}=0.3558326$.

These results are presented at most at the specific times given. These are not necessarily the times at which the solutions have settled to a steady state but are, however, simply representative times at which the qualitative characteristics of the solutions are now well defined and more-or-less uniform. Steady-state solutions come much later, for example, if we employ the following parameter list: $\alpha=1$, $G_c=G_s=1$, $\delta_{c_2}=0.1$, $\delta_{s_2}=1.0$, $\delta_{c_3}=0.1$, $\delta_{s_3}=0.1$, $De=0.4$, $Pr_c=0.6$, $Pr_s=12$, $Re_c=0.3$, $Re_s=100$, $\gamma=0.5$, $\beta=0.5$, $\varepsilon_\lambda=0.1$, $\varepsilon_{\eta_c}=0.1$, $\varepsilon_{\eta_s}=0.1$, $\varepsilon_s=0.1$, $\mathrm{d}t=0.0001$, on a 20×20 mesh in both the core and shell regions, we obtain the results shown in the table below:

	$t=1$	$t=3$	$t=15$	$t=20$	$t=25$	$t=30$
Max T_c at core outlet	0.00083	0.00175	0.00175	0.00175	0.00175	0.00175
Avg T_c at core outlet	0.00057	0.00090	0.00117	0.00117	0.00117	0.00117
Max T_s at shell outlet	0.19852	0.29670	0.30336	0.30336	0.30336	0.30336
Avg T_s at shell outlet	0.17189	0.25963	0.27292	0.27292	0.27292	0.27292

DOI: 10.1002/fld

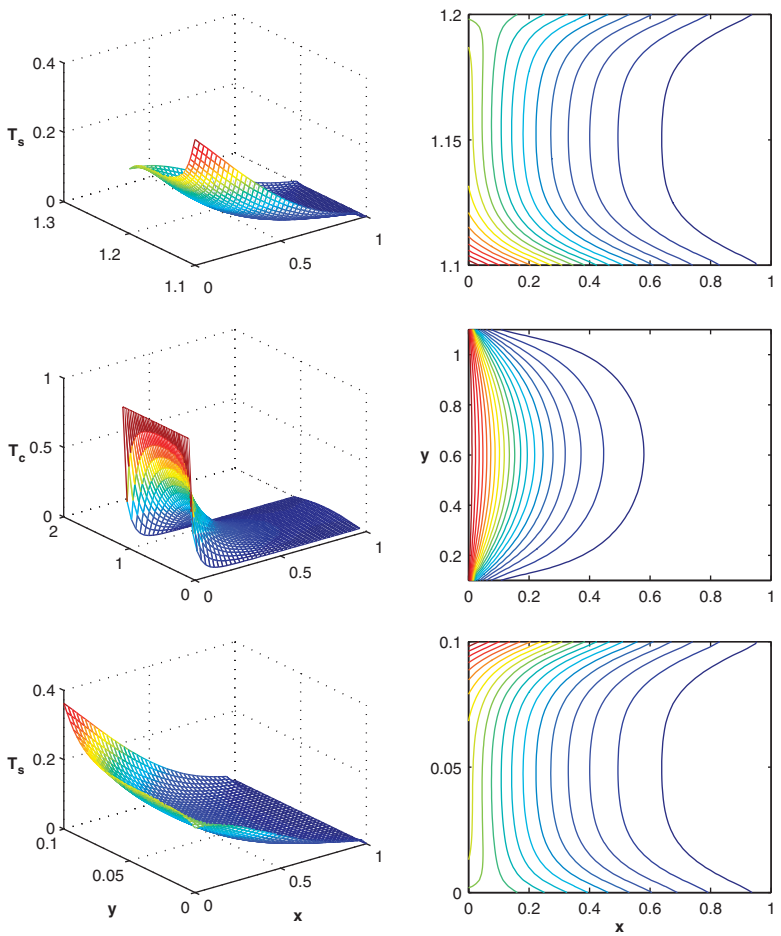

Figure 5. Surface and contour plots of temperature.

4.2. *Physical considerations*

In the physical setup, a heat exchanger with a square core would not only be unrealistic but also inefficient. The width is normally made a lot smaller than the length to improve efficiency and performance. With a large length to width ratio, however, spurious instabilities develop in our computational algorithm and an extensive stability analysis traces these instabilities back to the pressure equation. However, flows in such narrow horizontal pipes are usually specified with negligible transverse pressure variations, i.e. $\nabla p_c = (-G_c, 0)$. This condition removes the need to solve the pressure equation (11) and simply adds the term $-G_c$ on the right-hand side (and explicit part) of Equation (7). The resultant computational algorithm works stably for the required (small) values of ε_c. The graphical results are qualitatively the same as those already given for the square geometry. Taking $\varepsilon_c = 0.2$ and $\alpha = 1$, $G_c = G_s = 1$, $\delta_{c_2} = 0.1$, $\delta_{s_2} = 1.0$, $\delta_{c_3} = 0.1$, $\delta_{s_3} = 0.1$, $De = 0.4$, $Pr_c = 0.8$, $Pr_s = 2$, $Re_c = 0.6$, $Re_s = 100$, $\gamma = 0.5$, $\beta = 0.5$, $\varepsilon_\lambda = 0.1$, $\varepsilon_{\eta_c} = 0.1$, $\varepsilon_{\eta_s} = 0.1$, $\varepsilon_s = 0.1$, $\mathrm{d}t = 0.0001$, on a 30×30 mesh and at $t = 1$; we obtain max T_c, avg T_c, max T_s and avg T_s, respectively,

DOI: 10.1002/fld

as 0.00169, 0.00092, 0.32879, 0.24178. The corresponding Newtonian problem comparably gives 0.00169, 0.00092, 0.32872, 0.24177, respectively. Thus, unlike [22] where drastic differences were noted in comparisons between Newtonian and viscoelastic fluid behavior in shear flows subjected to chemical reactions, the current results show relatively comparable behavior between such fluids.

5. CONCLUSION

We have successfully modeled and numerically solved the conducto-convective heat transfer between Newtonian shell-side and Giesekus core-side liquids in straight double-pipe counterflow heat exchangers. Our results show that a viscoelastic core-fluid leads to slightly higher (but practically comparable) temperature drops within the core-fluid compared with the use of a corresponding Newtonian fluid. We have also checked our codes for both temporal and mesh convergence.

ACKNOWLEDGEMENTS

This research was carried out under a Postdoctoral Research Fellowship at the Center for Advanced Studies in Mathematics (CASM) at Lahore University of Management Sciences (LUMS). The author thanks CASM for financial and material support and is also most grateful to the reviewers for their insightful comments.

REFERENCES

1. Butterworth D. Developments in shell-and-tube heat exchangers. In *New Developments in Heat Exchangers*, Afgan N, Carvalho M, Bar-Cohen A, Butterworth D, Roetzel W (eds). Gordon & Breach: New York, 1996; 437–447.
2. Holman JP. *Heat Transfer* (8th edn). McGraw-Hill: New York, 1997.
3. Saunders EAD. *Heat Exchangers*: *Selection*, *Design and Construction*. Wiley: New York, 1988.
4. Shah RK. Heat exchangers. In *Encyclopedia of Energy Technology and the Environment*, Bisio A, Boots SG (eds). Wiley: New York, 1994; 1651–1670.
5. Walker G. *Industrial Heat Exchangers*: *A Basic Guide* (2nd edn). Hemisphere Publishing: Washington, DC, 1990.
6. Rennie TJ. Numerical and experimental studies of a double-pipe helical heat exchanger. *Ph.D. Thesis*, McGill University, 2004.
7. Huang LY, Wen JX, Karayiannis TG, Mathews RD. CFD modelling of fluid flow and heat transfer in a shell and tube heat exchanger. *PHOENICS Journal of Computational Fluid Dynamics and its Applications* 1996; **9**(2):181–209.
8. Stevanović Z, Ilić G, Radojković N, Vukić M, Stefanović V, Vučković G. Design of shell-and-tube heat exchangers by using CFD technique—Part 1: thermo-hydraulic calculation. *Facta Universitatis*, *Series*: *Mechanical Engineering* 2001; **1**(8):1091–1105.
9. Bird RB, Curtiss CF, Armstrong RC, Hassager O. *Dynamics of Polymeric Liquids*, *Vol. 1*, *Fluid Mechanics* (2nd edn). Wiley: New York, 1987.
10. Ferry JD. *Viscoelastic Properties of Polymers* (3rd edn). Wiley: New York, 1981.
11. Wapperom P. Nonisothermal flows of viscoelastic fluids: thermodynamics analysis and numerical simulation. *Ph.D. Thesis*, Delft University of Technology, 1995.
12. Olagunju DO, Cook LP, McKinley GH. Effect of viscous heating on linear stability of viscoelastic cone-and-plate flow: axisymmetric case. *Journal of Non-Newtonian Fluid Mechanics* 2002; **102**(2):321–342.
13. Olagunju DO. Secondary flow in non-isothermal viscoelastic parallel-plate flow. *Journal of Engineering Mathematics* 2005; **51**:325–338.
14. Dressler M, Edwards BJ, Öttinger HC. Macroscopic thermodynamics of flowing polymeric liquids. *Rheologica Acta* 1999; **38**:117–136.

DOI: 10.1002/fld

15. Wapperom P, Hulsen MA, van der Zanden JPPM. A numerical method for steady and nonisothermal viscoelastic fluid flow for high Deborah and Péclet numbers. *Rheologica Acta* 1998; **37**:73–88.
16. Khomami B, Renardy Y, Su KC, Clarke MA. An experimental/theoretical investigation of interfacial stability in superposed pressure-driven channel flow of well-characterized viscoelastic fluids. Part II: nonlinear stability. *Journal of Non-Newtonian Fluid Mechanics* 2000; **91**:85–104.
17. Chinyoka T, Renardy YY, Renardy M, Khismatullin DB. Two-dimensional study of drop deformation under simple shear for Oldroyb-B liquids. *Journal of Non-Newtonian Fluid Mechanics* 2005; **31**:45–56.
18. Chinyoka T. Numerical simulation of stratified flows and droplet deformation in 2D shear flow of Newtonian and viscoelastic fluids. *Ph.D. Thesis*, Virginia Polytechnic Institute and State University, 2004. Available from: http://scholar.lib.vt.edu/theses/available/etd-11292004-130236/.
19. Li J, Renardy YY, Renardy M. A numerical study of periodic disturbances in two-layer Couette flow. *Physics of Fluids* 1998; **10**(12):3056–3071.
20. Renardy Y, Renardy M, Chinyoka T, Khismatullin DB, Li J. A viscoelastic VOF-PROST code for the study of drop deformation. *ASME Heat Transfer/Fluids Engineering Summer Conference*, *HTFED2004*, Charlotte, North Carolina, U.S.A., 11–15 July 2004; CDROM Track 5, 56114.pdf.
21. Chorin J. A numerical method for solving incompressible viscous flow problems. *Journal of Computational Physics* 1967; **2**:12–26.
22. Chinyoka T. Computational dynamics of a thermally decomposable viscoelastic lubricant under shear. *Journal of Fluids Engineering* (ASME) 2008; in press.

DOI: 10.1002/fld